Yin et al. Nanoscale Res Lett (2021) 16:11
https://doi.org/10.1186/s11671-020-03469-9

Nanoscale Research Letters

NANO EXPRESS

Open Access

Cobalt Phosphide (Co_2P) with Notable Electrocatalytic Activity Designed for Sensitive and Selective Enzymeless Bioanalysis of Hydrogen Peroxide

Donghang Yin[1], Junyan Tang[1], Rongbiao Bai[1], Shuyi Yin[1], Mengnan Jiang[1], Zigui Kan[1], Hongmei Li[1], Fei Wang[1*] and Caolong Li[1,2*]

Abstract

In this work, cobalt phosphide nanoparticles (Co_2P NPs) were prepared by simple and mild hydrothermal method without the use of harmful phosphorous source. The morphological structure and surface component of Co_2P were characterized by transmission electron microscopy, X-ray diffraction and X-ray photoelectron spectroscopy measurements. Considering the excellent electrocatalytic reduction activity and good electrical conductivity of transition-metal phosphide, we fabricated Co_2P NPs on indium tin oxide (ITO) substrate (Co_2P/ITO) for H_2O_2 detection. The Co_2P/ITO transducer displayed a rapid amperometric response less than 5 s, a broader response range from 0.001 to 10.0 mM and a low detection limit of 0.65 μM. In addition, the non-enzymatic Co_2P/ITO sensor showed outstanding selectivity, reproducibility, repeatability and stability, all of which qualified the Co_2P/ITO electrode for quite a reliable and promising biosensor for H_2O_2 sensing.

Keywords: Cobalt phosphide, Hydrogen peroxide, Non-enzymatic, Amperometric sensor

Introduction

Hydrogen peroxide (H_2O_2) is a representative reactive oxygen species in living organisms, and it plays a critical role in normal physiologic function [1]. The concentration of H_2O_2 in living cells is related closely with the cell physiological balance [2]. Numerous studies have also been reported that cancer, Alzheimer's diseases, Parkinson's diseases and some severe diseases may be caused by abnormal concentration of H_2O_2 [3–5]. Developing accurate, sensitive, rapid and selective methods to detect the concentration of H_2O_2, a normal oxidative stress biomarker, will be undoubtedly beneficial to the early diagnosis. Up to now, a host of analytical methods such as spectroscopy [6], colorimetry [7], fluorescence [8, 9] and electrochemical methods [10–12] have been applied in H_2O_2 determination. Electrochemical method, especially amperometric test is gradually becoming one of the most simple and effective detection methods for H_2O_2 biological analysis among diverse sensing methods due to its advantages such as high sensitivity, outstanding selectivity and low cost.

Enzymatic electrochemical sensors have been proved to be effective instruments for detecting H_2O_2. However, the large-scale practical application of enzyme-based sensors is limited by complicated immobilization, environmental instability and low reproducibility. Therefore, developing non-enzymatic electrochemical H_2O_2 sensors is highly indispensable.

In recent years, a growing number of sensors based on noble metal [13–15], non-noble metal and their

*Correspondence: feiwang@cpu.edu.cn; licl@cpu.edu.cn
[1] Key Laboratory of Biomedical Functional Materials, School of Science, China Pharmaceutical University, Nanjing 211198, People's Republic of China
Full list of author information is available at the end of the article

corresponding compounds [16–19] or carbon materials [20, 21] have been used for electrochemical H_2O_2 detection. As electrochemical active materials for fabricating non-enzymatic biosensors, transition metal compounds have been received increasing interests. Transition-metal phosphides (TMPs) are a class of newly developed materials with excellent electrocatalytic activity, good electrical conductivity and a plenty of outstanding properties. Thus, they have been extensively studied for applications in water splitting [22, 23], hydrodesulfurization [24], and supercapacitor electrodes [25]. Recent research indicates that CoP, Ni_2P and Cu_3P [26–28] can also be used as efficient electrocatalyst for non-enzymatic H_2O_2 detection. However, the number of researches about the application of TMPs in bioanalysis is still limited nowadays. Besides, the use of triphenylphosphine [29, 30], white phosphorous [31, 32] or other environmental hazardous phosphorous source [33] can increase the operational risk in the preparation of TMPs. Therefore, some research work for developing green method in TMP preparation is worth being supplemented in this area.

In this work, cobalt phosphide nanoparticles (Co_2P NPs) were prepared by one-step hydrothermal method utilizing cobalt acetate and red phosphorous as raw materials. Herein, we fabricated Co_2P NPs on indium tin oxide (ITO) substrate by drop-casting method for H_2O_2 detection. Co_2P displayed excellent electrocatalytic activity toward H_2O_2 reduction. Moreover, it revealed favorable selectivity, excellent reproducibility and good stability, which therefore exhibited its potential application as a sensitive platform for H_2O_2 detection.

Experimental Section

Reagents and Materials

All reagents were analytical grade and used without further purification. Cobalt (II) acetate tetrahydrate ($Co(Ac)_2{\cdot}4H_2O$), cobalt chloride hexahydrate ($CoCl_2{\cdot}6H_2O$), D-(+)-glucose, L-Glycine (L-Gly), ascorbic acid (AA), uric acid (UA), urea, NaCl, KCl, NaH_2PO_4, Na_2HPO_4, hydrogen peroxide (30% H_2O_2), ethanol and acetone were purchased from Sinopharm Chemical Reagent Co., Ltd. China. D-(−)-fructose, L-arginine (L-Arg), L-lysine (L-Lys), dopamine (DA), acetaminophen (APAP), amino trimethylene phosphonic acid (ATMP, 50 wt%) were purchased from Aladdin Ltd. Commercial red phosphorous (98.5%, 100 mesh) were purchased from Energy Chemical Technology (Shanghai) Co., Ltd. Nafion PFSA polymer dispersion (5%) were purchased from Beijing Honghaitian technology Co., Ltd. Deionized water was used in all the experiments. The indium tin oxide (ITO) glass ($10 \times 20 \times 1.1$ mm with an ITO film of 185 ± 2 nm and a sheet resistance of 6.6 ± 0.1 Ω) was supplied from Shenzhen South Xiangcheng Technology Co., Ltd.

Synthesis of Co_2P Nanoparticles

Commercial red phosphorous (2 g) was dispersed in 15 mL H_2O under sonification and hydrothermally treated at 200 °C for 12 h in a 50 mL Teflon-lined stainless autoclave to clear oxide layers [34]. Then, the hydrothermal treated red phosphorous was dried in a vacuum oven. After finishing the pretreatment of red phosphorous, 1 mmol $Co(Ac)_2{\cdot}4H_2O$ was dissolved in 30 mL distilled water to obtain an aqueous solution. Then, the hydrothermal treated red phosphorous was added into the solution under ultrasonication for 15 min with the molar ratio of Co/P 1/10. The prepared suspension was rapidly poured into a 50 mL Teflon-lined autoclave. Then, the autoclave was placed in an electronic oven and hydrothermally treated at 160, 200, 240 °C for 12 h, respectively. Then, the product was collected by centrifugation and washed three times with distilled water and ethanol, respectively. Finally, Co_2P NPs were dried at 60 °C for 3 h in air.

Synthesis of $Co(PO_3)_2$

The preparation method of $Co(PO_3)_2$ was referred to the previous report [35]. 0.1 M $CoCl_2{\cdot}6H_2O$ methanol solution was prepared firstly. Then, 2 mL ATMP (50 *w*t%) was added dropwise into 20 mL the above purple solution and stirred for 30 min. The insoluble cobalt-metaphosphate coordination polymer formed in the solution subsequently. The obtained pink powder was further heated to 900 °C under Ar flow with a heating rate of 5 °C·min^{-1} and then held for 2 h. After cooling down to room temperature, the black product was collected and reheated at 650 °C for 4 h in air to remove the carbonized organic ligand. Finally, the light-purple powder of $Co(PO_3)_2$ was obtained.

Fabrication of Co_2P/ITO Electrode

Firstly, the ITO glass (1 cm × 2 cm) was cleaned in acetone, ethanol and deionized water for 10 min, respectively, by sonication. After that, the treated ITO was dried under nitrogen sweeping. For the modification of the electrode, 5 mg of the Co_2P NPs was dispersed in 1 mL deionized water to form 5 mg mL^{-1} Co_2P suspension. Then, 5 μL 5% Nafion solution was added into the suspension and the mixture was ultrasonicated for 15 min to obtain uniform ink-like suspension. The Co_2P/ITO electrode was prepared by drop-casting 100 μL of Co_2P suspension on the ITO surface, and dried in air as working electrode. The schematic preparation process of Co_2P/ITO electrode is shown in Scheme 1.

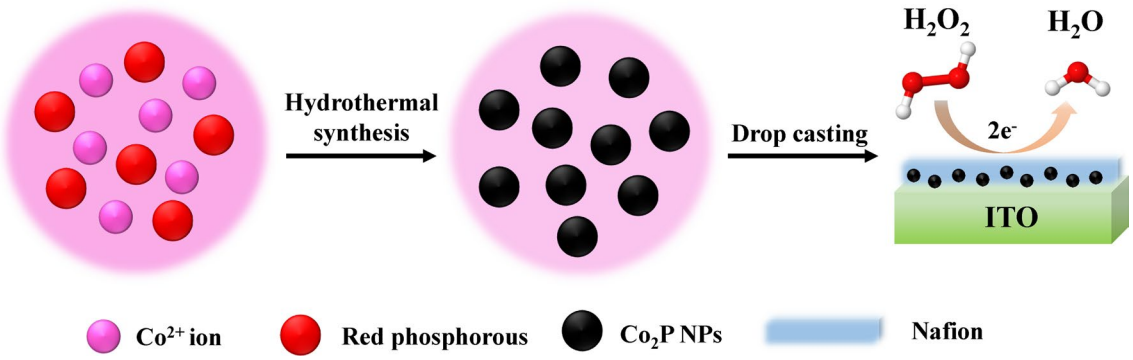

Scheme 1. Schematic preparation of Co_2P/ITO electrode and H_2O_2 sensing

Characterizations

The X-ray diffraction (XRD) data were analyzed by a D8 ADVANCE diffractometer with Cu Kα radiation. The transmission electron microscopy (TEM) measurement was conducted using a Tecnai G2 F20 with energy dispersed spectrum detector. X-ray photoelectron spectroscopy (XPS) spectra were measured on a Thermo ESCALAB 250XI spectrometer.

Electrochemical Measurements

Voltammetry measurements were accomplished by CHI 660E electrochemical workstation in a three-electrode system, employing Co_2P/ITO electrode as working electrode, a platinum foil (1 cm × 1 cm) as counter electrode and Ag/AgCl with 3 M KCl solution as reference electrode to study the electrochemical activities of the synthesized samples for H_2O_2 detection. Phosphate buffer saline (PBS; 0.1 M, pH 7.4) was used as the electrolyte to simulate the physiological medium in human body. The sensing performances of Co_2P/ITO electrode toward H_2O_2 detection were investigated by cyclic voltammetry (CV) and amperometry (I-t). All the detection experiments were performed under 100 rpm stirring at room temperature. Electrochemical impedance tests were performed on VersaSTAT 3F electrochemical workstation and ferricyanide solution was used as the electrolyte for impedance measurement.

Results and Discussion

Characterization of Co_2P NPs

The crystal structure of Co_2P NPs was confirmed by XRD measurement. Figure 1a shows the XRD patterns of Co_2P samples prepared at 160, 200 and 240 °C for 12 h. The Co_2P sample prepared at 200 °C shows diffraction peaks at around 40.7°, 40.9°, 52.0° and 56.2° which correspond to the characteristic diffraction planes at (121), (201), (002) and (320) for the orthorhombic phase of Co_2P (JCPDS no. 32-0306). When temperature varied from 160 to 200 °C, the intensities of diffraction peaks increased and the peaks became narrower and sharper, indicating that the products had a higher crystallinity at 200 °C. However, when temperature reached 240 °C, some impurities were formed and the diffraction peaks at 29.7° was attributed to the diffraction plane at (-222) of $Co(PO_3)_2$ (JCPDS no. 27-1120). The influence of synthetic time on the preparation of Co_2P under 200 °C is shown in Additional file 1: Fig. S1. When the time duration was controlled within 12 h, the obtained Co_2P NPs displayed the lowest value of full width at half maximum of (121) peak, suggesting better crystallinity. Besides, none of impurities existed in the sample when the reaction time varied from 6 to 24 h. According to the Scherrer formula, the calculated grain size of Co_2P NPs prepared at 200 °C for 12 h was 14.2 nm.

The morphology of Co_2P NPs was assessed by TEM measurements. As shown in Fig. 1b, the product prepared at 200 °C is composed of irregular nanoparticles with the diameter around 10–20 nm and two lattice fringes can be clearly seen in the high-resolution TEM (HRTEM) image (inset in Fig. 1b). The distance between the neighboring planes is 0.22 nm, corresponding to the (121) facets of Co_2P, which further confirms that the formation of TMP is Co_2P.

The XPS technique was employed in analyzing the chemical compositions on the surface of the Co_2P. Additional file 1: Fig. S2 shows the XPS survey spectrum of Co_2P. Co, P and O elements are detected in the sample, confirming the existence of Co_2P and some oxidized products. Energy-dispersive X-ray spectroscopy (EDX) spectra of Co_2P (Additional file 1: Fig. S3) further confirms the co-existence of three elements (Co, P, O) in the sample. The high-resolution XPS spectra of Co 2p and P 2p are shown in Fig. 1c, d, respectively. In Co 2p spectrum, the peaks at 781.1 and 797.6 eV can be ascribed to

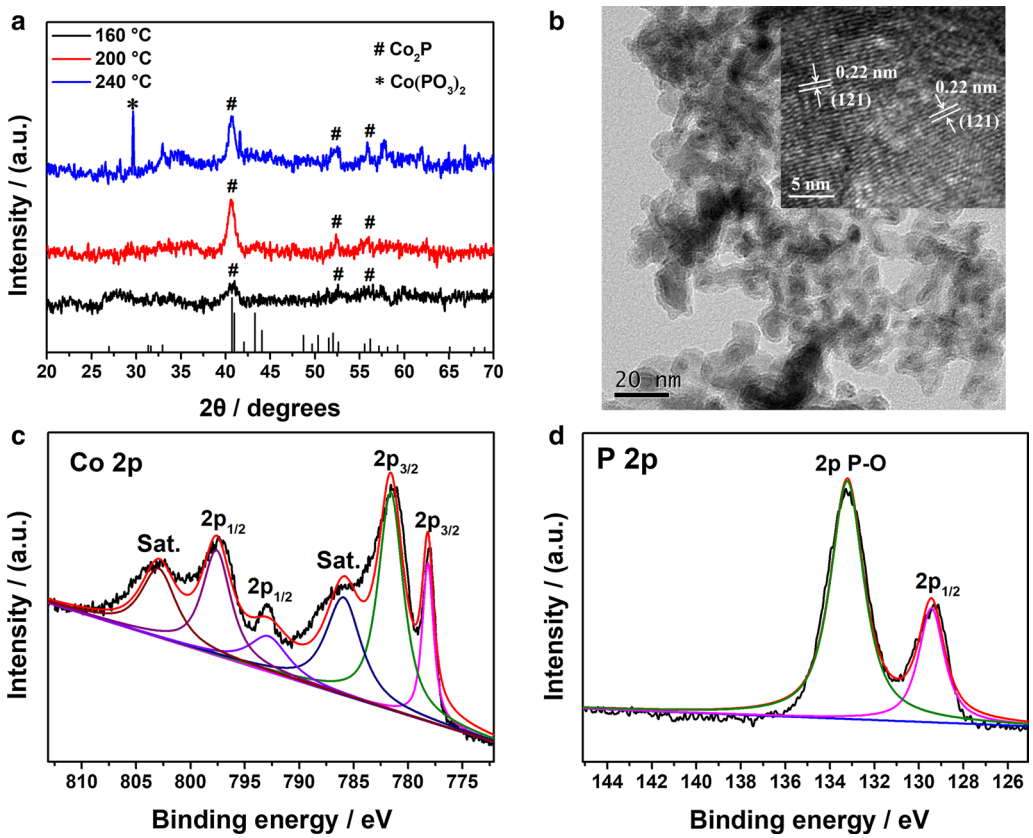

Fig. 1 **a** XRD patterns of Co_2P NPs prepared at different temperatures for 12 h. **b** Transmission electron microscopic image and high-resolution transmission electron microscopic image (inset) of Co_2P NPs. XPS spectra of Co_2P in the **c** Co 2*p* region and **d** P 2*p* region

the binding energies (BEs) of Co^{2+} $2p_{3/2}$ and Co^{2+} $2p_{1/2}$, respectively [26, 36]. The peaks at 786.0 and 803.1 eV are two apparent shake-up satellite peaks. The Co 2p BE of 778.2 eV shifts positively from that of metallic Co (777.9 eV), which suggests that Co in Co_2P has a partial positive charge (δ^+) with a small value ($0<\delta<2$) [37]. On the contrary, the P 2*p* BE of 129.4 eV shifts negatively from that of elemental P (130.2 eV) so that the P has a partial negative charge (δ^-) in Co_2P. The changes of BE in Co and P element compared with their elementary substance, respectively, reveal that the transfer direction of electron density in Co_2P is from Co to P [38]. Superficial oxidation of Co_2P generates a few of oxidized P species in the sample. Therefore, the peaks at 133.2 eV in high BE range are assigned to the oxides [39].

Electrochemical Detection of H_2O_2 at Co_2P/ITO Electrode

To investigate the electrocatalytic activity of Co_2P NPs in H_2O_2 reduction, we designed a non-enzymatic H_2O_2 electrode by drop-casting Co_2P NPs suspension on a bare ITO surface. Figure 2a shows the CV curves of bare ITO and Co_2P/ITO in 0.1 M PBS at pH 7.4 with and without 5.0 mM H_2O_2, respectively. The dash lines indicate that the response of bare ITO to H_2O_2 reduction is negligible. However, the Co_2P/ITO electrode exhibits a remarkable reduction peak at − 0.5 V in the presence of H_2O_2, which demonstrates the prominent electrocatalytic activity of Co_2P NPs toward H_2O_2 reduction. Figure 2b presents the CV curves of Co_2P/ITO at different scan rates (from 30 to 100 mV s^{-1}) with 2.5 mM H_2O_2. When increasing the scan rate, the reduction peak current increased and the peak potential shifted to the more negative potential side, indicating the reduction in H_2O_2 on Co_2P/ITO was an irreversible reaction. The corresponding calibration curve (inset, Fig. 2b) shows that the reduction peak current densities increase linearly proportional to the scan rate, suggesting that the electrochemical reduction of H_2O_2 on the surface of Co_2P/ITO electrode is a surface-controlled process [40].

Figure 2c, d show the amperometric response and the calibration curve of Co_2P/ITO electrode upon the successive addition of H_2O_2 into the 0.1 M PBS at − 0.5 V with stirring. The Co_2P/ITO electrode exhibited quick response to the addition of H_2O_2 and achieved the steady-state current within 5 s. The calibration curve in Fig. 2d shows that the transducer displays a multi-linear

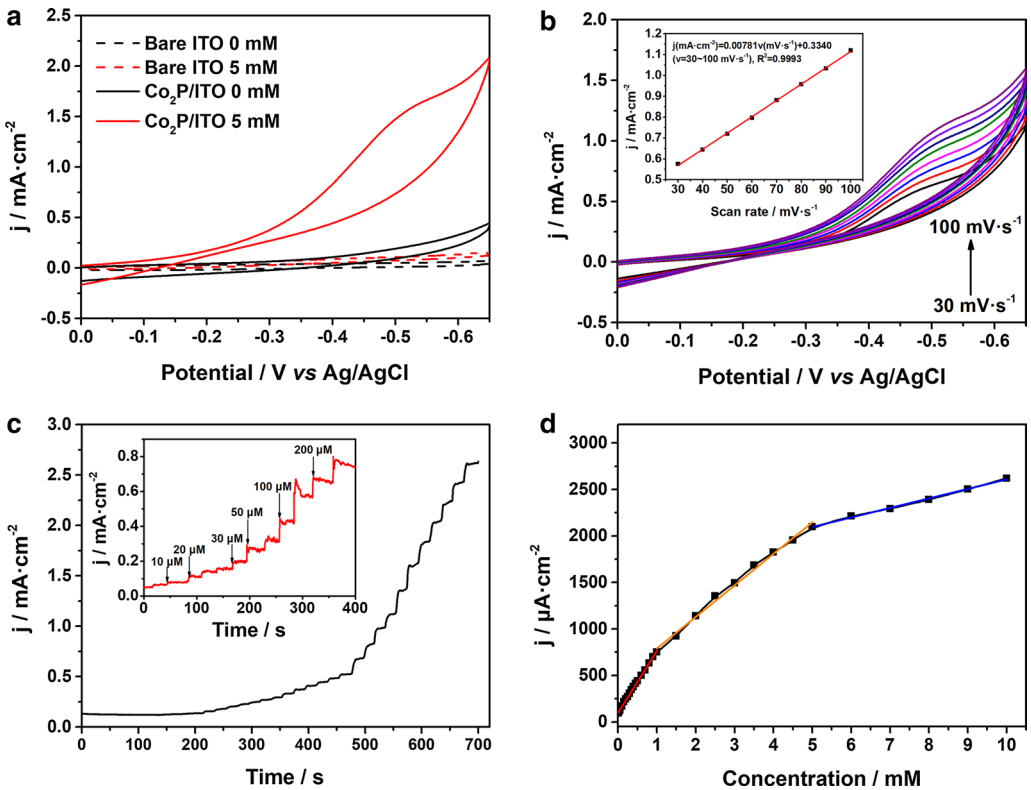

Fig. 2 **a** CV curves of bare ITO and Co_2P/ITO electrode in 0.1 M PBS with and without 5.0 mM H_2O_2 at a scan rate of 100 mV s^{-1}. **b** CV curves of Co_2P/ITO electrode in 2.5 mM H_2O_2 at scan rates from 30 to 100 mV s^{-1}. Inset: The corresponding plot of current versus the scan rate. **c** Amperometric responses of Co_2P/ITO electrode with successive addition of H_2O_2 in 0.1 M PBS. **d** The calibration curve of steady current versus the concentration of H_2O_2

range of H_2O_2 concentration from 0.001 to 1.0 mM, 1.0–5.0 mM and 5.0–10.0 mM. The sensitivity of the sensor alters with the increasing concentration of H_2O_2, due to the change of electrocatalytic reduction kinetics of H_2O_2 on the electrode surface. According to previous reports, the rate-determining step of H_2O_2 reduction is dominated by H_2O_2 adsorption at low concentration, whereas the activation of H_2O_2 is the major determinant at high concentration. In the middle region, the reduction kinetics of H_2O_2 is controlled by adsorption and activation at the same time [10]. A multitude of analysts will adsorb on the surface of Co_2P and cover the active sites in the high concentration, which lead to the decrease in sensitivity [41].

The comparison on H_2O_2 sensing performances of the prepared Co_2P sample at various reaction temperature and time is shown in Additional file 1: Fig. S4, S5 and Table S1, indicating that the Co_2P sample prepared at 200 °C for 12 h displays the best H_2O_2 sensing performances. When reaction temperature raised to 240 °C, the formed $Co(PO_3)_2$ in Co_2P could be regarded as impurity. To further clarify the influence of $Co(PO_3)_2$ on H_2O_2 detection, the electrochemical properties of $Co(PO_3)_2$ were investigated. As shown in Additional file 1: Fig. S6, $Co(PO_3)_2$ displays negligible electrochemical response toward H_2O_2 and its conductivity is inferior to Co_2P, which declines the current signal of Co_2P/ITO in amperometric test. Therefore, the higher purity and better crystallinity of Co_2P sample may contribute to the improvement of sensing performances. Thus, we choose the Co_2P sample prepared at 200 °C and 12 h as the best H_2O_2 sensing material. The calibration *I–t* curve also presents a good linear relationship in the concentration of 1.0–50 μM, the physiological range of H_2O_2 concentration in biosystem (Fig. S7) [28], which could be helpful to improve the possibility of practical applications of this sensor. In addition, the limit of detection (LOD) of the H_2O_2 sensor can be calculated to be 0.65 μM at a signal-to-noise ratio of 3. Compared with the previously reported H_2O_2 sensor, the comprehensive electrochemical performances of our Co_2P/ITO transducer are superior to those with favorable sensitivity, linear range and LOD, as shown in Table 1.

Table 1 Sensing performances on comparison of Co_2P/ITO with other cobalt-based non-enzymatic H_2O_2 sensors

Materials	Linear range	Sensitivity (μA mM^{-1} cm^{-2})	Detection limit (μM)	References
Co_3O_4–rGO	15–675 μM	1140	2.4	[42]
Co_3O_4 nanowire/N-carbon foam	0.01–1.4 mM	230	1.4	[16]
Co_3O_4/MWCNTs	0.02–0.43 mM	1000	2.46	[43]
Co_3O_4/rGO	1–18.5 mM	–	0.5	[44]
CoS	0.005–14.82 mM	459	1.5	[45]
CoP NWs	0.001–12 mM	–	0.48	[26]
Hb/CoP-CC (carbon cloth)	2.0–2670 μM	56.2	0.67	[40]
Co_2P/ITO	0.0001–1.0 mM	668.6	0.65	This work
	1.0–5.0 mM	339.0		
	5.0–10.0 mM	102.3		

After detecting 1.0 mM H_2O_2 repeatedly for 35 times (Fig. 3a, b), the XPS spectra in Co 2*p* and P 2*p* region of Co_2P are analyzed to further investigate the sensing mechanism. There is no significant change in the position of the peaks in P 2*p* region before and after H_2O_2 detection. However, the peaks at 778.2 and 793.0 eV in Co 2*p* spectrum disappeared after multiple measurements. As the peak at 778.2 eV indicates the existence of reduced Co species in Co_2P sample [37], the disappearance of these two peaks demonstrates that the reduced Co species with low valence in Co_2P may be oxidized by H_2O_2 during the detection process, especially with high concentration of H_2O_2. The remnant peaks in Co 2*p* region (782.1 and 798.3 eV) are attributed to Co^{2+} $2p_{3/2}$ and Co^{2+} $2p_{1/2}$, respectively, suggesting the exclusive existence of Co(II) species in Co_2P after multiple measurements. According to previous reports about the utilization of cobalt-based electrocatalyst in H_2O_2 detection, Co^{2+} species are demonstrated as the catalytic active sites for H_2O_2 reduction [46–48]. Generally, the electrochemical reduction in H_2O_2 goes through two steps in PBS [49, 50], as shown below.

$$H_2O_2 + e^- \rightarrow OH_{ad} + OH^- \quad (1)$$

$$OH_{ad} + e^- \rightarrow OH^- \quad (2)$$

$$2OH^- + 2H^+ \rightarrow 2H_2O \quad (3)$$

In the first step, H_2O_2 obtains an electron to form adsorbed OH^- (OH_{ad}). When the intermediate OH_{ad} obtains an additional electron, the final reduction product of H_2O_2, H_2O, is generated. As the redox potential of H_2O_2/H_2O is higher than Co^{3+}/Co^{2+}, the Co(II) species in Co_2P can be oxidized to Co(III) in the electron transfer process and H_2O_2 is reduced to H_2O irreversibly. During the amperometric test, the applied bias is − 0.5 V versus Ag/AgCl (equals to 0.14 V vs. NHE), which is lower than the standard redox potential of Co^{3+}/Co^{2+}. As a result, the oxidized Co(III) can be reduced to Co(II)

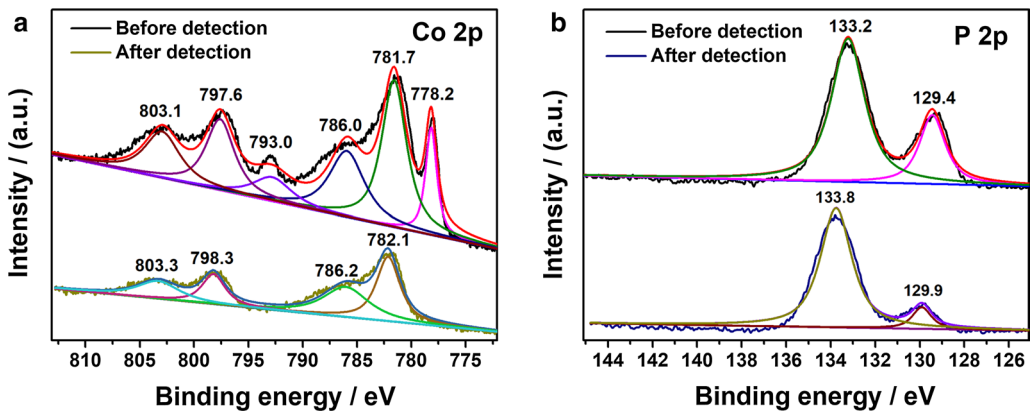

Fig. 3 The comparison of XPS spectra in **a** Co 2*p* region and **b** P 2*p* region of Co_2P before and after detection

and theses catalytic active sites of Co(II) are regenerated again. Therefore, it can be concluded that the catalytic cycle of Co (II) species takes place during electrochemical detection of H_2O_2 and the reduced Co species with low valence are oxidized by H_2O_2 after repetitive measurements.

Selectivity, Stability, Reproducibility and Repeatability of Co_2P/ITO Electrode

Anti-interference performance is another important property of biosensor. High purity nitrogen was utilized to avoid the influence by dissolved oxygen in solution because oxygen could be reduced at similar potential which was applied in amperometric test [51]. Comparing the CV curves of Co_2P/ITO in 0.1 M PBS with or without nitrogen purging, the reduction potential and the current response of 2.5 mM H_2O_2 are similar, as shown in Fig. S8, which therefore suggests that the interference of dissolved oxygen can be neglected. Selectivity of Co_2P/ITO was also tested with common substances and other small molecules in body fluid, such as some inorganic salts, saccharides, amino acids and reductive biomolecules. As shown in Fig. 4a, the current response after adding the above interferents can be neglected compared with the response of 1.0 mM H_2O_2. As both two O atoms of H_2O_2 could be bonded with one or two Co atoms [52], the H_2O_2 molecule would chemically adsorb on Co(II) species in Co_2P specifically. In addition, the interference from indiscriminate oxidation of some reductive compounds in real biological samples at high potential can be also reduced significantly at lower bias potential [53]. Therefore, the favorable selectivity of Co_2P toward H_2O_2 mainly benefits from the Co(II) species as specific adsorption sites and the applied negative bias potential during sensing process.

Moreover, the stability, reproducibility and repeatability of the Co_2P/ITO transducer were also evaluated. The reduction peak currents of ten successive scanning CV curves in 50 μM H_2O_2 is shown in Fig. 4b. After ten cycles, the peak current of the electrode only fell by 2.7%. In addition, the sensor remained about 98.2% of its initial current response after being stored in air for one month (Fig. S9), demonstrating ideal detecting stability and outstanding long-term durability. The electrode-to-electrode

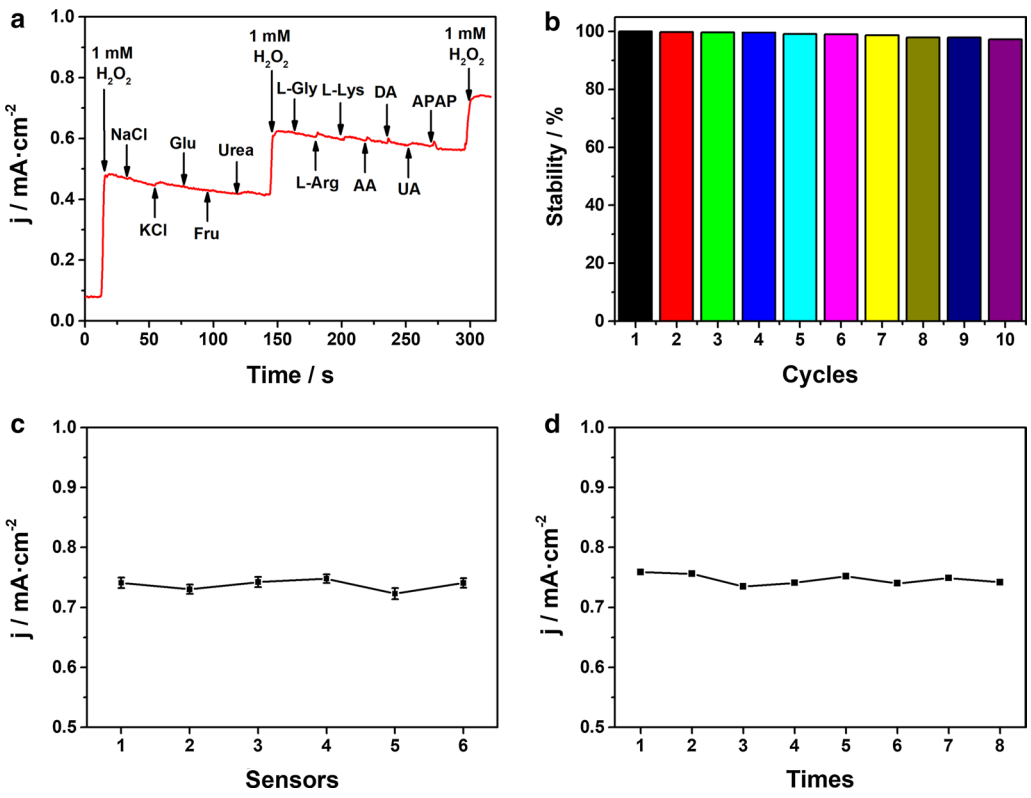

Fig. 4 **a** Amperometric responses of Co_2P/ITO electrode with the addition of 1 mM H_2O_2 and other interfering species (10 mM NaCl, KCl, Glu, Fru, urea, L-Gly, L-Arg, L-Lys, AA; 1 mM DA, UA; 0.5 mM APAP) in 0.1 M PBS. **b** The cathodic peak currents of ten successive scanning CV curves in 50 μM H_2O_2. **c** Reproducibility of six Co_2P/ITO electrodes for detecting 1.0 mM H_2O_2. **d** Repeatability of Co_2P/ITO electrode for detecting 1.0 mM H_2O_2 eight times

reproducibility is investigated by calculating the relative standard deviation (RSD) of H_2O_2 current responses. To eliminate the potential error from electrode fabrication as far as possible, the steady current density in the presence of H_2O_2 is subtracted by the initial background signal of individual electrode and the obtained difference value is regarded as the electrochemical response of each electrode. Six Co_2P/ITO electrodes were fabricated under the same conditions for controlled experiments and the RSD of current responses was 1.24%, as shown in Fig. 4c, indicating the relatively excellent reproducibility of Co_2P/ITO. Meanwhile, repeatability was measured in one electrode by detecting 1.0 mM H_2O_2 eight times, and the RSD of 1.14% was achieved (Fig. 4d). The above results illustrate the satisfactory stability, reproducibility and repeatability of the electrode for non-enzymatic electrochemical detection of H_2O_2.

Conclusion

In summary, Co_2P NPs were successfully synthesized by hydrothermal method. Furthermore, the Co_2P NPs prepared at 200 °C for 12 h have been proved as an efficient catalyst toward electrochemical reduction of H_2O_2 in pH 7.4 PBS. As a non-enzymatic H_2O_2 sensor, the Co_2P/ITO electrode displayed a rapid amperometric response less than 5 s, a broader response range from 0.001 to 10.0 mM and a low detection limit of 0.65 μM, as well as satisfactory selectivity, reproducibility and stability. This work aims to broaden the research about the application of transition metal phosphide in electrochemical detection of small biomolecules and our Co_2P/ITO sensor could be designed as a new non-enzymatic platform for H_2O_2 detection.

Supplementary information

The online version contains supplementary material available at https://doi.org/10.1186/s11671-020-03469-9.

Additional file 1. **Fig. S1.** XRD patterns of Co_2P NPs synthesized with different reaction times at 200 °C. **Fig. S2.** XPS survey spectrum of Co_2P. **Fig. S3.** EDX spectra of Co_2P NPs. **Fig. S4.** Amperometric responses of Co_2P/ITO electrodes prepared at (a) different temperatures and (c) different times with successive addition of H_2O_2 in 0.1 M PBS. (b), (d) The calibration curve of steady current versus the concentration of H_2O_2. **Fig. S5.** The linear relationship between current density and concentration of H_2O_2 in different concentration ranges (a) 0.0001–1.0 mM, (b) 1.0–5.0 mM, (c) 5.0–10.0 mM. **Fig. S6.** Comparison of electrochemical properties between Co_2P and $Co(PO_3)_2$. (a) LSV curves of Co_2P and $Co(PO_3)_2$ modified electrode in 0.1 M PBS with and without 2.5 mM H_2O_2 at a scan rate of 100 mV s^{-1}. (b) Nyquist plots of bare ITO, Co_2P/ITO and $Co(PO_3)_2$/ITO electrode (electrolyte: 5.0 mM $K_3[Fe(CN)_6]$/ $K_4[Fe(CN)_6]$ and 0.1 M KCl; bias: open circuit potential, amplitude: 5 mV, frequency range: 100 kHz ~ 0.01 Hz). **Fig. S7.** The linear relationship between current density and concentration of H_2O_2 in the physiological range. **Fig. S8.** CVs for Co_2P/ITO electrode in 0.1 M PBS with or without N_2 purging at a scan rate of 100 mV s^{-1}. **Fig. S9.** CV responses at a scan rate of 100 mV s^{-1} in 0.1 M PBS containing 0.1 mM H_2O_2 of a Co_2P/ITO electrode before and after being stored in air for one month. **Table S1**. The comparison on H_2O_2 sensing performance of the bare ITO electrode and the prepared Co_2P sample at various reaction temperature.

Abbreviations

NPs: Nanoparticles; ITO: Indium tin oxide; TEM: Transmission electron microscopy; HRTEM: High-resolution transmission electron microscopy; XRD: X-ray diffraction; XPS: X-ray photoelectron spectroscopy; EDX: Energy-dispersive X-ray spectroscopy; CV: Cyclic voltammetry; I-t: Amperometry; Gly: Glycine; AA: Ascorbic acid; UA: Uric acid; Arg: Arginine; Lys: Lysine; DA: Dopamine; APAP: Acetaminophen; ATMP: Trimethylene phosphonic acid; PBS: Phosphate buffer; LOD: Detection limit; RSD: Relative standard deviation.

Acknowledgements

Not applicable.

Authors' contributions

The manuscript was written through contributions of all authors. DHY, JYT and RBB designed and performed the experiments. JYT and SYY analyzed the experiment data and wrote the manuscript. MNJ and HML assisted with interpretation of the data from electrochemical test. ZGK, FW and CLL helped to check the manuscript before submission. CLL conceived of the study and all authors read and approved the final version of the manuscript.

Funding

We appreciate the financial support by the National Natural Science Foundation of China (81660708), National Key Research and Development Project (2019YFC0312602), Science and Technology Support Program of Jiangsu Province (BE2018389) and the Key Project of Tibetan Medical Administration of Tibet (2017005). The work is also supported by "Double First-Class" University Project (CPU2018GY25), the Qinglan Project of Young Academic Leaders of Jiangsu Province and Fundamental Research Funds for the Central Universities (2632019YX01).

Availability of data and materials

All data and materials are fully available without restriction.

Competing interests

The authors declare that they have no competing interests.

Author details

[1] Key Laboratory of Biomedical Functional Materials, School of Science, China Pharmaceutical University, Nanjing 211198, People's Republic of China. [2] Tibetan Medicine Research Institute, Tibetan Traditional Medical College, Lhasa 850000, Tibet, People's Republic of China.

Received: 25 June 2020 Accepted: 20 December 2020
Published online: 13 January 2021

References

1. Rhee SG (2006) H_2O_2, a necessary evil for cell signaling. Science 312:1882–1883
2. Lippert AR, De Bittner GCV, Chang CJ (2011) Boronate oxidation as a bioorthogonal reaction approach for studying the chemistry of hydrogen peroxide in living systems. Acc Chem Res 44:793–804
3. Finkel T, Serrano M, Blasco MA (2007) The common biology of cancer and ageing. Nature 448:767–774
4. Lux CD, Joshi-Barr S, Nguyen T, Mahmoud E, Schopf E, Fomina N, Almutairi A (2012) Biocompatible polymeric nanoparticles degrade and release cargo in response to biologically relevant levels of hydrogen peroxide. J Am Chem Soc 134:15758–15764
5. Rossi DJ, Jamieson CHM, Weissman IL (2008) Stems cells and the pathways to aging and cancer. Cell 132:681–696
6. Gasser C, Kilgus J, Harasek M, Lendl B, Brandstetter M (2018) Enhanced mid-infrared multi-bounce ATR spectroscopy for online detection of hydrogen peroxide using a supercontinuum laser. Opt Express 26:12169–12179

7. Guo JL, Wang Y, Zhao M (2018) 3D flower-like ferrous(II) phosphate nanostructures as peroxidase mimetics for sensitive colorimetric detection of hydrogen peroxide and glucose at nanomolar level. Talanta 182:230–240
8. Feng CC, Wang FY, Dang YJ, Xu ZA, Yu HJ, Zhang W (2017) A self-assembled ratiometric polymeric nanoprobe for highly selective fluorescence detection of hydrogen peroxide. Langmuir 33:3287–3295
9. Lampard EV, Sedgwick AC, Sun XL, Filer KL, Hewins SC, Kim G, Yoon J, Bull SD, James TD (2018) Boronate-based fluorescence probes for the detection of hydrogen peroxide. Chemistryopen 7:262–265
10. Huang JF, Zhu YH, Zhong H, Yang XL, Li CZ (2014) Dispersed CuO nanoparticles on a silicon nanowire for improved performance of nonenzymatic H_2O_2 detection. ACS Appl Mater Interfaces 6:7055–7062
11. Li DP, Liu XY, Yi R, Zhang JX, Su ZQ, Wei G (2018) Electrochemical sensor based on novel two-dimensional nanohybrids: MoS_2 nanosheets conjugated with organic copper nanowires for simultaneous detection of hydrogen peroxide and ascorbic acid. Inorg Chem Front 5:112–119
12. Liu J, Bo XJ, Yang J, Yin DD, Guo LP (2017) One-step synthesis of porphyrinic iron-based metal-organic framework/ordered mesoporous carbon for electrochemical detection of hydrogen peroxide in living cells. Sens Actuators B Chem 248:207–213
13. Bai ZH, Li GY, Liang JT, Su J, Zhang Y, Chen HZ, Huang Y, Sui WG, Zhao YX (2016) Non-enzymatic electrochemical biosensor based on Pt NPs/RGO-CS-Fc nano-hybrids for the detection of hydrogen peroxide in living cells. Biosens Bioelectron 82:185–194
14. Wang XJ, Guo XL, Chen J, Ge C, Zhang HY, Liu YY, Zhao L, Zhang Y, Wang ZM, Sun LT (2017) Au nanoparticles decorated graphene/nickel foam nanocomposite for sensitive detection of hydrogen peroxide. J Mater Sci Technol 33:246–250
15. Liu W, Hiekel K, Hubner R, Sun HJ, Ferancova A, Sillanpaa M (2018) Pt and Au bimetallic and monometallic nanostructured amperometric sensors for direct detection of hydrogen peroxide: Influences of bimetallic effect and silica support. Sens Actuators B Chem 255:1325–1334
16. Dong JK, Xu HY, Zhang FJ, Chen C, Liu L, Wu GT (2014) Synergistic effect over photocatalytic active Cu_2O thin films and their morphological and orientational transformation under visible light irradiation. ApplCatal A Gen 470:294–302
17. Sherino B, Mohamad S, Halim SNA, Manan NSA (2018) Electrochemical detection of hydrogen peroxide on a new microporous Ni-metal organic framework material-carbon paste electrode. Sens Actuators B Chem 254:1148–1156
18. Xue B, Li KZ, Gu SY, Zhang LL, Lu JH (2018) Ni foam-supported ZnO nanowires and Co_3O_4/$NiCo_2O_4$ double-shelled nanocages for efficient hydrogen peroxide detection. Sens Actuators B Chem 262:828–836
19. Yuan RM, Li HJ, Yin XM, Zhang LL, Lu JH (2018) Stable controlled growth of 3D CuO/Cu nanoflowers by surfactant-free method for non-enzymatic hydrogen peroxide detection. J Mater Sci Technol 34:1692–1698
20. Fu L, Wang AW, Lai GS, Lin CT, Yu JH, Yu AM, Liu Z, Xie KF, Su WT (2018) A glassy carbon electrode modified with N-doped carbon dots for improved detection of hydrogen peroxide and paracetamol. Microchim Acta 185:87
21. Huang B, Wang Y, Lu ZW, Du HJ, Ye JS (2017) One pot synthesis of palladium-cobalt nanoparticles over carbon nanotubes as a sensitive non-enzymatic sensor for glucose and hydrogen peroxide detection. Sens Actuators B Chem 252:1016–1025
22. Yan LT, Cao L, Dai PC, Gu X, Liu DD, Li LJ, Wang Y, Zhao XB (2017) Metal-organic frameworks derived nanotube of nickel-cobalt bimetal phosphides as highly efficient electrocatalysts for overall water splitting. Adv Funct Mater 27:1703455
23. Xin YM, Kan X, Gan LY, Zhang ZH (2017) Heterogeneous bimetallic phosphide/sulfide nanocomposite for efficient solar-energy-driven overall water splitting. ACS Nano 11:10303–10312
24. Song LM, Zhang SJ, Ma QY (2015) Synthesis of an iron phosphide catalyst based on sulfides and hydrodesulfurization property. Chem Eng J 281:281–285
25. Elshahawy AM, Guan C, Li X, Zhang H, Hu YT, Wu HJ, Pennycook SJ, Wang J (2017) Sulfur-doped cobalt phosphide nanotube arrays for highly stable hybrid supercapacitor. Nano Energy 39:162–171
26. Liu DN, Chen T, Zhu WX, Cui L, Asiri AM, Lu Q, Sun XP (2016) Cobalt phosphide nanowires: an efficient electrocatalyst for enzymeless hydrogen peroxide detection. Nanotechnology 27:33
27. Xiong XL, You C, Cao XQ, Pang LF, Kong RM, Sun XP (2017) Ni_2P nanosheets array as a novel electrochemical catalyst electrode for non-enzymatic H_2O_2 sensing. Electrochim Acta 253:517–521
28. Li ZZ, Xin YM, Wu WL, Fu BL, Zhang ZH (2016) Topotactic conversion of copper(I) phosphide nanowires for sensitive electrochemical detection of H_2O_2 release from living cells. Anal Chem 88:7724–7729
29. Chen XJ, Cheng M, Chen D, Wang RM (2016) Shape-controlled synthesis of Co_2P nanostructures and their application in supercapacitors. ACS Appl Mater Interfaces 8:3892–3900
30. Pan Y, Lin Y, Chen YJ, Liu YQ, Liu CG (2016) Cobalt phosphide-based electrocatalysts: synthesis and phase catalytic activity comparison for hydrogen evolution. J Mater Chem A 4:4745–4754
31. Ni Y, Li J, Zhang L, Yang S, Wei X (2009) Urchin-like Co_2P nanocrystals: synthesis, characterization, influencing factors and photocatalytic degradation property. Mater Res Bull 44:1166–1172
32. Liu SL, Yan L, Li HL (2014) Solvothermal synthesis of flower-like Co_2P nanostructures and its electrochemical performance. Sci Adv Mater 6:746–750
33. Pradhan B, Kumar GS, Dalui A, Khan AH, Satpati B, Ji QM, Shrestha LK, Ariga K, Acharya S (2016) Shape-controlled cobalt phosphide nanoparticles as volatile organic solvent sensor. J Mater Chem C 4:4967–4977
34. Xia DH, Shen ZR, Huang GC, Wang WJ, Yu JC, Wong PK (2015) Red Phosphorus: an earth-abundant elemental photocatalyst for "green" bacterial inactivation under visible light. Environ Sci Technol 49:6264–6273
35. Xu LH, Zhang SL, Guo SY, Zhang XJ, Cosnier S, Marks RS, Wang WJ, Zeng HB, Shan D (2020) ATMP derived cobalt-metaphosphate complex as highly active catalyst for oxygen reduction reaction. J Catal 387:129–137
36. Liang F, Huang L, Tian L, Li JY, Zhang HJ, Zhang SW (2018) Microwave-assisted hydrothermal synthesis of cobalt phosphide nanostructures for advanced supercapacitor electrodes. CrystEngComm 20:2413–2420
37. Huang ZP, Chen ZZ, Chen ZB, Lv CC, Humphrey MG, Zhang C (2014) Cobalt phosphide nanorods as an efficient electrocatalyst for the hydrogen evolution reaction. Nano Energy 9:373–382
38. Burns AW, Layman KA, Bale DH, Bussell ME (2008) Understanding the relationship between composition and hydrodesulfurization properties for cobalt phosphide catalysts. ApplCatal A Gen 343:68–76
39. Liu YW, Cao XQ, Kong RM, Du G, Asiri AM, Lu Q, Sun XP (2017) Cobalt phosphide nanowire array as an effective electrocatalyst for non-enzymatic glucose sensing. J Mater Chem B 5:1901–1904
40. Dong SY, Yang QX, Fu YL, Zhang DD, Huang TL (2018) Carbon cloth-supported cobalt phosphide as an active matrix for constructing enzyme-based biosensor. J Solid State Electr 22:1689–1696
41. Wang L, Yu J, Zhang YY, Yang H, Miao LF, Song YH (2017) Simple and large-scale strategy to prepare flexible graphene tape electrode. ACS Appl Mater Interfaces 9:9089–9095
42. Kong LJ, Ren ZY, Zheng NN, Du SC, Wu J, Tang JL, Fu HG (2015) Interconnected 1D Co_3O_4 nanowires on reduced graphene oxide for enzymeless H_2O_2 detection. Nano Res 8:469–480
43. Heli H, Pishahang J (2014) Cobalt oxide nanoparticles anchored to multiwalled carbon nanotubes: synthesis and application for enhanced electrocatalytic reaction and highly sensitive nonenzymatic detection of hydrogen peroxide. Electrochim Acta 123:518–526
44. Zhang XM, Li KZ, Li HJ, Lu JH, Fu QG, Zhang LL (2016) Hydrothermal synthesis of cobalt oxide porous nanoribbons anchored with reduced graphene oxide for hydrogen peroxide detection. J Nanopart Res 18:232
45. Wu WQ, Yu BB, Wu HM, Wang SF, Xia QH, Ding Y (2017) Synthesis of tremella-like CoS and its application in sensing of hydrogen peroxide and glucose. Mater Sci Eng C Mater 70:430–437
46. Chen Q, Ding R, Liu H, Zhou LX, Wang Y, Zhang Y, Fan GY (2020) Flexible active-site engineering of monometallic Co-layered double hydroxides for achieving high-performance bifunctional electrocatalyst toward oxygen evolution and H_2O_2 reduction. ACS Appl Mater Interfaces 12:12919–12929
47. Sun Y, Xu H, Zhao X, Hui ZY, Yu CY, Wang LM, Xue JL, Zhao Y, Zhou RC, Dai HH, Miao CY, Chen Q, Zhou JY, Sun Z, Huang W (2019) Identifying the active site of ultrathin NiCoLDH as an efficient peroxidase mimic with superior substrate affinity for sensitive detection of hydrogen peroxide. J Mater Chem B 7:6232–6237
48. Wang L, Wu T, Wu H, Zhong J, Wang N, Wang RM (2018) A novel non-enzymatic hydrogen peroxide sensor based on Co:ZnO modified electrodes. Prog Nat Sci Mater 28:24–27

49. Zhang W, Fan GZ, Yi H, Jia G, Li ZS, Yuan CW, Bai YF, Fu DG (2018) Interfacial engineering of hierarchical transition metal oxide heterostructures for highly sensitive sensing of hydrogen peroxide. Small 14:1703713
50. Zhang CM, Li L, Ju J, Chen W (2016) Electrochemical sensor based on graphene-supported tin oxide nanoclusters for nonenzymatic detection of hydrogen peroxide. Electrochim Acta 210:181–189
51. Meichtry JM, Dillert R, Bahnemann DW, Litter MI (2015) Application of the stopped flow technique to the TiO_2-heterogeneous photocatalysis of hexavalent chromium in aqueous suspensions: comparison with O_2 and H_2O_2 as electron acceptors. Langmuir 31:6229–6236
52. Lu JT, Zhang HW, Li S, Guo SS, Shen L, Zhou TT, Zhong H, Wu L, Meng QG, Zhang YX (2020) Oxygen-vacancy-enhanced peroxidase-like activity of reduced Co_3O_4 nanocomposites for the colorimetric detection of H_2O_2 and glucose. Inorg Chem 59:3152–3159
53. Jia WZ, Guo M, Zheng Z, Yu T, Rodriguez EG, Wang Y, Lei Y (2009) Electrocatalytic oxidation and reduction of H_2O_2 on vertically aligned Co_3O_4nanowalls electrode: toward H_2O_2 detection. J Electroanal Chem 625:27–32

Publisher's Note